

Predictive Motion Planning for AUVs subject to strong time-varying currents and forecasting uncertainties

Van T. Huynh, Matthew Dunbabin and Ryan N. Smith

Abstract— This paper presents a novel path planning method for minimizing the energy consumption of an autonomous underwater vehicle subjected to time varying ocean disturbances and forecast model uncertainty. The algorithm determines 4-Dimensional path candidates using Nonlinear Robust Model Predictive Control (NRMPC) and solutions optimised using A*-like algorithms. Vehicle performance limits are incorporated into the algorithm with disturbances represented as spatial and temporally varying ocean currents with a bounded uncertainty in their predictions. The proposed algorithm is demonstrated through simulations using a 4-Dimensional, spatially distributed time-series predictive ocean current model. Results show the combined NRMPC and A* approach is capable of generating energy-efficient paths which are resistant to both dynamic disturbances and ocean model uncertainty.

I. INTRODUCTION

Autonomous Underwater Vehicles (AUVs) are routinely used for extended missions ranging from environmental monitoring to surveillance [1]–[3]. To extend vehicle endurance there is an increasing focus on exploiting variations in ocean currents [4]–[6], with energy savings of over 32% demonstrated in strongly tidal conditions [7].

The key challenges in predictive path planning using ocean currents relate to the spatiotemporal variability in ocean current magnitude and direction, as well as the associated forecasting accuracy. Figure 1 illustrates such variability by showing the change in predicted ocean current over a 4-hour period in Moreton Bay, Queensland. As shown, the magnitude of current varies significantly in space and time, and in regions can exceed many AUV operational limits. These ocean currents can significantly affect both navigation performance and associated onboard power requirements. Furthermore, any forecasting uncertainties may lead to the executed trajectories significantly deviating from planned paths.

Therefore, optimal energy efficient path planning that is robust to variable and uncertain environmental conditions is required to increase the operational reliability of these vehicles. In this work, a Nonlinear Robust Model Predictive Control (NRMPC) method is proposed whose objective function minimizes the AUVs’ onboard power consumption whilst being robust to uncertainties.

V. Huynh is with the School of Electrical Engineering and Computer Science, Queensland University of Technology, 2 George Street, Brisbane, QLD 4000, Australia. e-mail: tv.huynh@qut.edu.au

M. Dunbabin is with the Institute for Future Environments, Queensland University of Technology, 2 George Street, Brisbane, QLD 4000, Australia. e-mail: m.dunbabin@qut.edu.au

R. Smith is with Department of Physics and Engineering, Fort Lewis College, Berndt Hall 603, 1000 Rim Drive, Durango, CO 81301 USA. e-mail: rsmith@fortlewis.edu

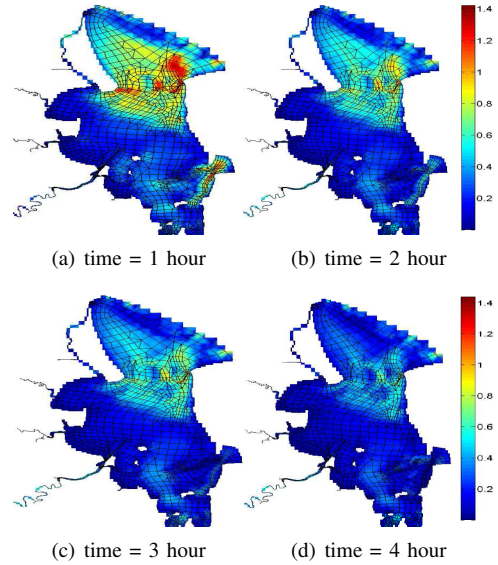


Fig. 1. Illustration of the spatial and temporal variability in ocean current magnitudes (m/s) over 4 hours for Moreton Bay, Australia. Ocean current predictions were generated by the Receiving Water Quality Model [8].

II. RELATED WORK

Path planning and execution for AUVs that take advantage of ocean currents is an active area of research. Garau [9] proposed a grid-based pregenerative large-scale AUV path planning which incorporates currents so as to obtain routes with minimum energy costs. Here, ocean currents are assumed two-dimensional and quasi-static, with the path constraint to grid nodes. Other grid-based and nongrid-based approaches to incorporate the dynamics of real ocean currents include A* [10], [11], level set [12], genetic algorithm [13], and anisotropic fast marching algorithm [14].

Time-dependent, continuous ocean model path-planning has been explored in [7], [15]–[17], with global search algorithms employed to solve optimization problems for minimal energy consumption of the vehicles. Even though these studies considered more realistic AUV operating environments, they all assume the ocean model predictions are perfect and deterministic. Additionally, they do not consider the spatiotemporal depth-dependent variation in ocean current in their planners.

To account for modelling uncertainty, Markov Decision Processes have been considered for minimum time path planning [18], and prediction of time and place for vehicle surfacing with minimal risk of collision [19]. However, they do not address the problem of minimum energy planning. NRMPC has been successfully employed to deal with model uncertainties and disturbances in path planning [20]. Whilst used for shorter duration trajectory planning (e.g. [21]),

it has not yet been applied to the large-scale 4D path planning for AUVs. NRMPC has qualities which can address vehicle limitations and model uncertainty, as well as adapt in time. However, there lacks standardized tools for searching solutions of the formulated NRMPC due to its nonlinearity, and mixtures of continuous and discrete variables resulting from the vehicle dynamics and ocean model predictions. Therefore, in this paper, we present A*-like algorithm that can be used to search for solutions of the NRMPC problem.

The remainder of the paper is structured as follows; Section III describes simplified models for an AUV subjected to ocean currents, Section IV presents NRMPC path planning methodology, with Section V describing the solver for the proposed NRMPC scheme. Finally, Section VI demonstrates the algorithms via simulation using real-ocean prediction data.

III. AUV KINEMATICS AND OCEAN MODELS

This section presents the mathematical models used in our analysis to describe the AUV and ocean dynamics.

A. Ocean Model

In this analysis it is assumed that the only disturbances acting on the AUV result from the 4-Dimensional (3 spatial and time) ocean currents. There are many models that can be used to predict ocean currents. In order to be model-independent, in this paper we generalise the representation of ocean currents as a series of 3-D matrices of current magnitude and direction with each matrix representing a prediction time-step.

In the algorithm verification described in this paper, the ocean current predictions were obtained from the Regional Ocean Modelling System (ROMS), produced at the Jet Propulsion Laboratory (JPL)-California Institute of Technology. ROMS is a split-explicit, free-surface, and topography-following-coordinate model. The model output has three nested horizontal configurations, with increasing resolution covering the US west coastal ocean (15 km), the southern California coastal ocean (5 km), and the Southern California Bight (2.2 km) [22]. ROMS also provides current prediction at 24 non-uniformly spaced depth bins from 0 m to 2000 m. ROMS provides this 4-Dimensional for the Southern California Bight data as hindcasts, nowcasts, and hourly forecasts (up to 72 hours) [23].

B. System model and control inputs

In this paper, the AUV is represented as a simplified 4-D kinematic model. Assuming sway, roll, and pitch motions are negligible, the vehicle's state relative to the inertial frame is defined by the vector $\boldsymbol{\eta} \triangleq (b_1, b_2, b_3, \psi)^\top$ consisting of the longitudinal (b_1), latitudinal (b_2), and vertical (b_3) (depth) coordinates, and heading angle (ψ). Additionally, \mathbf{v}_b is the body speed of the AUV in the direction of travel, \mathbf{v}_r is the AUV speed relative to the water, and $\mathbf{v}_a = (\dot{b}_1, \dot{b}_2, \dot{b}_3)^\top$ is the AUV absolute speed relative to the sea bottom. These velocities are graphically depicted in Fig. 2.

The ocean current velocities are represented by $\mathbf{v}_c = (v_{cb1}, v_{cb2}, v_{cb3})^\top$ along each inertial coordinate.

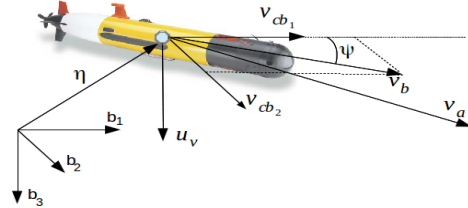


Fig. 2. Illustration of the AUV kinematics showing inertial frame coordinates (b_1, b_2, b_3, ψ), body-fixed velocity (\mathbf{v}_b), and ocean currents (\mathbf{v}_c).

In this analysis, it is assumed the body velocity \mathbf{v}_b and the relative velocity \mathbf{v}_r are varied to keep $\|\mathbf{v}_a\|$ constant. Therefore, the relative velocity is defined by $\mathbf{v}_r = \mathbf{v}_a - \mathbf{v}_c$.

The internal control inputs to the AUVs are $\mathbf{u} \triangleq (v_b, u_v, \psi)^\top$, where u_v is the input control for the heave (vertical) motion of the vehicle.

C. Continuous-time representation

Using the above notation, the corresponding equations of motion can be written as:

$$\begin{aligned} \dot{b}_1 &= v_b \cos \psi + v_{cb1}, \\ \dot{b}_2 &= v_b \sin \psi + v_{cb2}, \\ \dot{b}_3 &= \dot{u}_v + v_{cb3}. \end{aligned} \quad (1)$$

The vertical currents in this analysis are assumed to be negligible (i.e., $v_{cb3} = 0$). In this work we assume the vertical control action is instantaneous; hence, this results in $b_3 = u_v$. Future work will consider the case of non-negligible vertical currents and finite dive times.

Equation (1) can be considered a continuous system with state variable $\boldsymbol{\eta}$, control input \mathbf{u} , and disturbances \mathbf{v}_c . However, if there are predictions of the disturbances (e.g. ocean model) then these can be additional control inputs to the system. This results in the system having two forms of control actions; (1) the internal control \mathbf{u} , and (2) the external control \mathbf{v}_c . Therefore, Eq. (1) can be written as:

$$\dot{\boldsymbol{\eta}} = \begin{pmatrix} \cos \psi & 0 & 1 & 0 \\ 0 & \sin \psi & 0 & 1 \end{pmatrix} \begin{pmatrix} v_b \\ v_b \\ v_{cb1} \\ v_{cb2} \end{pmatrix}, \quad (2a)$$

$$b_3 = u_v, \quad (2b)$$

where $\bar{\boldsymbol{\eta}} = (b_1, b_2)^\top$ is the state variable representing positions of the vehicle in the horizontal plane.

D. Discrete-time representation

Given the sample time interval (T), Eq. (2a) can be expressed in discrete-time as:

$$\begin{aligned} \bar{\boldsymbol{\eta}}(k+1) &= \bar{\boldsymbol{\eta}}(k) + \begin{pmatrix} T \cos \psi & 0 \\ 0 & T \sin \psi \end{pmatrix} \begin{pmatrix} v_b \\ v_b \end{pmatrix} \\ &+ \begin{pmatrix} T & 0 \\ 0 & T \end{pmatrix} \begin{pmatrix} v_{cb1} \\ v_{cb2} \end{pmatrix}. \end{aligned} \quad (3)$$

Therefore, the state-space representation of the system is:

$$\bar{\boldsymbol{\eta}}(k+1) = f(\bar{\boldsymbol{\eta}}(k), \mathbf{U}(k)), \quad (4a)$$

$$b_3(k) = u_v(k), \quad (4b)$$

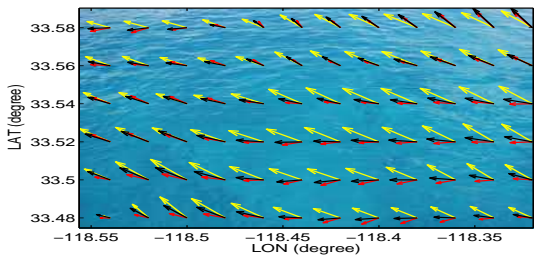


Fig. 3. Forecasting uncertainties of ocean currents where yellow, red, and black arrows are hindcasts, forecast, and nowcasts, respectively. Produced using ROMS data for the Southern California Bight from March 1-15, 2010.

where,

$$\begin{aligned} f(\bar{\eta}(k), U(k)) &= A(k)\bar{\eta}(k) + B(k)U(k), \\ A &= I_{2 \times 2}, \\ B(k) &= \begin{pmatrix} T \cos \psi & 0 & T & 0 \\ 0 & T \sin \psi & 0 & T \end{pmatrix}, \\ \text{and } U(k) &= (v_b, v_b, v_{cb_1}, v_{cb_2})^\top. \end{aligned}$$

E. Model uncertainties

Ocean model output contains predictions of both current magnitude and direction. In reality these predictions may not always match actual currents perfectly. Figure 3 illustrates the prediction performance of ROMS from 48 and 24 out from the nowcast. It can be seen that both the directions and magnitudes of long-term forecasted ocean currents vary considerably from the nowcast.

Nonetheless, we can observe that vectors of ocean currents from hindcasts, forecasts, and nowcasts span within some local regions around the nowcast vectors. Here it is assumed that predicted vectors of ocean currents at a particular coordinate lie within a bounded polytope. This restricts our path planning problem to one with bounded uncertainties.

Consequently, the equations of motion (2) can be rewritten to incorporate uncertainties such that:

$$\bar{\eta}(k+1) = A(k)\bar{\eta}(k) + B(k)U(k) + W\omega(k), \quad (5)$$

where $\omega(k) \in \mathbb{R}^{2 \times 1}$ is the uncertainty at time k , and $W = I_{2 \times 2} \in \mathbb{R}^{2 \times 2}$. As uncertainty has been incorporated into the model, the predicted ocean currents in $B(k)$ are nominal values. Estimating the size of the uncertainty polytope is outside the scope of this paper. Refer to [24] for details.

IV. PLANNING STRATEGY

In this work, a model predictive control methodology is proposed whose control inputs are the vehicles internal velocities and heading angle as well as the ocean model prediction. The technique determines the execution path for effective navigation in dynamic environments with minimal energy and robustness to uncertainties. The motion planning problem is to select the admissible control inputs for the vehicle that minimizes power consumption, respond to disturbances and uncertainties, and predict system states for predetermined steps ahead.

Nonlinear Robust Model Predictive Control (NRMPC) is proposed due to: (1) it can counteract uncertainties existing in the kinematic model (Eq. (2)), (2) the feed-back loop can comprise the observed uncertainties, and (3) it has the ability to explicitly account for hard constraints.

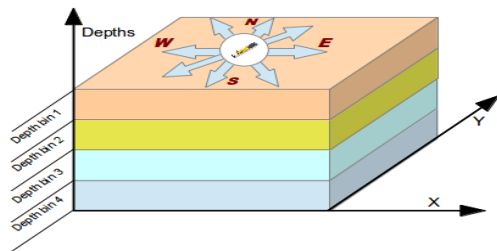


Fig. 4. Representation of set of internal control inputs. Possible states are restricted in this study to 8 possible horizontal directions at each of the discretised depth layers (bins).

A. NRMPC Problem Description

We will first define the NRMPC problem for the deterministic case, that is the ocean currents are assumed accurate.

Problem Statement 1: Given a start point η_0 and the goal point η_f , at each sampling time t_n , $n = 0, 1, 2, \dots$:

- 1) Measure the state $\eta(n) \in \mathcal{X}$ of the system.
- 2) Set $\eta_0 := \eta(n)$, solve the optimal control problem

$$\text{minimize } J_N(\eta_0, \mathbf{u}(\cdot)) := \sum_{k=0}^{N-1} \ell(\eta_{\mathbf{u}}(k, \eta_0), \mathbf{u}(k)),$$

with respect to $\mathbf{u}(\cdot) \in \mathbb{U}(\eta_0)$, subject to

$$\begin{aligned} \eta_{\mathbf{u}}(0, \eta_0) &= \eta_0, \\ \eta_{\mathbf{u}}(N, \eta_0) &\in \mathcal{B}_{\eta_f, r_f}, \\ \eta_{\mathbf{u}}(k+1, \eta_0) &= f(\eta_{\mathbf{u}}(k, \eta_0), \mathbf{u}(k)), \end{aligned}$$

and denote the obtained optimal control sequence by $\mathbf{u}^*(\cdot) \in \mathbb{U}(\eta_0)$.

- 3) Define the NRMPC-feedback value $\mu_N(\eta(n)) := \mathbf{u}^*(0) \in \mathcal{U}$ and use this control value in the next sampling period.

Here, \mathcal{X} and \mathbb{U} are sets of possible states and control inputs respectively. ℓ is a cost function. J_N is the total cost of the system predicted N steps ahead. $\eta_{\mathbf{u}}(k, \eta_0)$ represents the predictive state at k epochs ahead of an initial state η_0 and subject to a sequence of control inputs $\mathbf{u}(k)$. $f(\cdot)$ is the function representing Eq. (5).

State constraint: possible states of the system \mathcal{X} are the configuration space \mathcal{Q} . In the horizontal plane, the configuration space consists of all possible horizontal positions, yaw angle, and time. In the vertical direction, it consists of the predefined depth layers defined by the ocean model output (See Section III-A). Therefore, the configuration space can be represented as $\mathcal{Q} = \text{SE}(3) \times \mathbb{R}$

Input constraint: the set of possible control inputs \mathbb{U} contains a combination of continuous and discontinuous values. Particularly, the heading angle (ψ) is assumed here to be limited to one of eight predetermined directions ($\{N, NE, E, SE, S, SW, W, NW\}$) as depicted in Fig. 4. A larger number of directions introduces more states for consideration during optimization process, albeit resulting in a smoother returned path. u_v is control action that guides the vehicle along the vertical direction from the sea surface to maximum model depth. It is assumed the vehicle has the capability to dive to this maximum depth. Finally, the relative and absolute velocities are related via $v_r = v_a - v_c$.

Terminal constraint: The terminal constraint requires that the final state of the system $\eta_{\mathbf{u}}(N, \eta_0)$ under the control

sequence \mathbf{u} must stay within the ball $\mathcal{B}_{\eta_f, r_f}$. The value of r_f can be predetermined based on the navigational accuracy of the AUV.

Cost function: the cost function ℓ represents the energy consumed by the AUV at the time k under the control action \mathbf{u} and is defined as:

$$\ell = \ell_{hotel} + \ell_{energy} + \ell_{heuristic}, \quad (6)$$

where ℓ_{hotel} is the hotel load of the AUV¹, ℓ_{energy} is the energy required to attain \mathbf{v}_r , and $\ell_{heuristic}$ is an estimated energy to navigate from the current position to the destination.

The hotel load of the AUV is determined by the vehicle specific hotel energy per sample time constant ($E_{ht/sample}$) such that:

$$\ell_{hotel}(k) = kE_{ht/sample}. \quad (7)$$

The energy consumed by the vehicle to overcome the inertia and drag forces $F_{inertia}$ and F_{drag} is defined as,

$$\ell_{energy} = T(F_{inertia} + F_{drag})\|\mathbf{v}_r\|. \quad (8)$$

Similar to [7], we assume the vehicle dynamics are much faster than the prediction step and is in steady state motion such that $F_{inertia} = 0$ and the energy term becomes:

$$\ell_{energy}(k) = T(c_d\|\mathbf{v}_r(k)\|^3), \quad (9)$$

where c_d is a longitudinal drag coefficient of the AUV. In practice, these parameters are empirically derived.

Finally, the heuristic term ($\ell_{heuristic}$) is the estimated remaining energy required by the AUV to travel from the current position to the prespecified end node. This term is defined as:

$$\ell_{heuristic}(k) = \frac{\|\boldsymbol{\eta}(k) - \boldsymbol{\eta}_f\|}{\max\|\mathbf{v}_c + \mathbf{v}_r\|} E_{appr}, \quad (10)$$

where $\boldsymbol{\eta}_f$ is the final position of the AUV, and E_{appr} is an approximate, minimum energy per sampling time consumed by the vehicle at each time step. The denominator of Eq. (10) is an estimation of maximum absolute speed the vehicle might attain around the setpoint absolute speed. The introduction of $\ell_{heuristic}$ into the total cost (ℓ) assists searching in an A*-based algorithm for the NRMPC solution. The fact that Eq. (10) contains ratio of the Euclidean distance between the field point and the desired goal and the estimation of maximum absolute speed aims to guarantee the heuristic cost will be lower than the actual cost to reach the end point from the given position. This further assists the A*-based algorithm to search for optimal or near-optimal solutions.

We now consider the situation whereby ocean current predictions have forecasting inaccuracies which are spanned inside uncertainty polytopes. To increase robustness against uncertainty, we formulate the NRMPC in the form of a min-max optimization problem, that is the minimum path with maximum cost within the uncertainty polytope, such that:

Problem Statement 2: Given the initial point $\boldsymbol{\eta}_0$ and the goal destination $\boldsymbol{\eta}_f$, at each sampling time t_n , $n = 0, 1, 2, \dots$,

¹The hotel load is the constant power consumed to operate the vehicle's computing and sensor systems independent of propulsion.

- 1) Measure the state $\boldsymbol{\eta}(n) \in \mathcal{X}$ of the system.
- 2) Given

$$J_N := \sum_{k=0}^{N-1} \ell(\boldsymbol{\eta}(k), \mathbf{u}(k), \boldsymbol{\omega}(k)). \quad (11)$$

Set $\boldsymbol{\eta}_0 := \boldsymbol{\eta}(n)$, solve the optimal control problem,

$$\min_{\mathbf{u}(k)} \max_{\boldsymbol{\omega}(k)} J_N(\boldsymbol{\eta}_0, \mathbf{u}(\cdot), \boldsymbol{\omega}(\cdot))$$

with respect to $\mathbf{u}(\cdot) \in \mathbb{U}(\boldsymbol{\eta}_0)$, subject to

$$\boldsymbol{\eta}_{\mathbf{u}}(0, \boldsymbol{\eta}_0) = \boldsymbol{\eta}_0,$$

$$\boldsymbol{\eta}_{\mathbf{u}}(N, \boldsymbol{\eta}_0) \in \mathcal{B}_{\eta_f, r},$$

$$\boldsymbol{\eta}_{\mathbf{u}}(k+1, \boldsymbol{\eta}_0) = f(\boldsymbol{\eta}_{\mathbf{u}}(k, \boldsymbol{\eta}_0), \mathbf{u}(k), \boldsymbol{\omega}(k)),$$

and denote the obtained optimal control sequence by $\mathbf{u}^*(\cdot) \in \mathbb{U}(\boldsymbol{\eta}_0)$.

- 3) Define the NRMPC-feedback value $\mu_N(\boldsymbol{\eta}(n)) := \mathbf{u}^*(0) \in \mathcal{U}$ and use this control value in the next sampling period.

Using this min-max optimization formulation is inspired by [25]. Instead of solving the problem with nominal values, the total energy expended by the vehicle is bounded by the worst cases at every time epoch. The nominal case of the problem can be considered as a situation of which predicted current vectors are situated at the center of the uncertain polytopes. Contrary to this case, the worst cases of the problem are situations of which predicted current vectors are pointing to vertices of the uncertain polytopes. Hence, min-max problem is equivalent to finding the minimal of the worst case costs. Using this method, we assure that the actual total energy of the system will never exceed the predicted total energy even though there exists uncertainties in the ocean model.

V. SOLVING THE NRMPC PROBLEM

In this analysis, we assume that currents, even under the worst conditions, in the area of interest do not exceed the maximum-achievable speed of the AUV. As such, the area of interest is considered fully-controllable, and convergence of the planned paths is guaranteed. Once this assumption is satisfied, the process of searching for solutions of NRMPC can be undertaken.

The NRMPC problem formulated in Section IV is a nonlinear mixed integer optimization problem as the model kinematic constraint is nonlinear and ψ and u_v are considered discrete values over a sample time. However, the problem is now complicated since it needs to be solved in the min-max framework. Most optimisation tools for NRMPC consider separately the unconstrained nonlinear optimization, and mixed-integer linear optimization [26], [27]. Consequently, we propose an optimization scheme based on the A* algorithm that is able to search a solution for this NRMPC problem.

A. Execution of the NRMPC planner

The structure of the proposed integrated planner and controller based on nonlinear model predictive control and system kinematic model is shown in Fig. 5. The block diagram illustrates methodology proposed in Section IV whereby at each sampling time (t_n) the NRMPC is solved

to plan an energy-optimal path from η_o to η_f . The return of the optimizer is a prediction of states and control inputs for N steps ahead. The first element of the predicted control inputs will be assigned to the AUV as control input at time t_n . This process is repeated until the AUV reaches the goal destination.

Algorithm 1 presents the implementation of the NRMPC scheme shown in Fig. 5. Algorithm 1 uses *GenerateTimeNode* to initialize nodes \mathbf{x}_{start} and \mathbf{x}_{end} based on the locations of initial and target waypoints. Here \mathbf{x}_{start} is the first node of a tree G whose vertices set is V and edge set is E . Each node of G contains information about system state $(b_1(k), b_2(k), b_3(k), \psi(k))^T$ of the AUV, control input \mathbf{u} to reach the node's state, and an associated cost J . Similar to A* method [28], Algorithm 1 has an open list \sqsupset containing the unexplored states, and a closed list \wp containing the explored ones.

Algorithm 1, through the use of *ConnectionCheck* determines whether \mathbf{x}_{start} and \mathbf{x}_{end} can connect directly with each other, and return a *path* if they are connectible. Otherwise, the main loop of the algorithm is executed, and firstly checks whether the current prediction step exceeds the predetermined horizon N , or if *flag* signals satisfaction of the terminal constraint. If not, the function *ExploreTree* (See Algorithm 2) is invoked to build an A*-like tree. Finally, *FindMinPath* is used to extract a minimal-cost path from \mathbf{x}_{start} to \mathbf{x}_{end} .

Algorithm 1: NRMPC solution searching algorithm

Input: Initial and target waypoints $\bar{\eta}_0 = \{b_{1o}, b_{2o}\}$, $\bar{\eta}_f = \{b_{1f}, b_{2f}\}$, ROMS, and termination ball $\mathcal{B}_{\bar{\eta}_f, r_f}$.

Output: Control sequence $\mathbf{u}(k) = (u_b(k), u_v(k), \psi(k))^T$.

- 1 $\mathbf{x}_{start} \leftarrow \text{GenerateTimeNode}(\bar{\eta}_0)$
- 2 $\mathbf{x}_{end} \leftarrow \text{GenerateTimeNode}(\bar{\eta}_f)$
- 3 $V \leftarrow \{\mathbf{x}_{start}\}; E \leftarrow \emptyset; G \leftarrow (V, E)$
 $\sqsupset \leftarrow \mathbf{x}_{start}; \wp = [];$
- 4 **if** *ConnectionCheck*($\mathbf{x}_{start}, \mathbf{x}_{end}, r_f$) **then**
- 5 | *path* $\leftarrow \{\mathbf{x}_{start}; \mathbf{x}_{end}\}$
- 6 **else**
- 7 | /* Building and exploring tree if number of horizons not reached or terminal constraint not established */
- 8 | **while** ($k \leq N$ or *flag* == 0) **do**
- 9 | | [G, flag] \leftarrow *ExploreTree*($G, \mathbf{x}_{end}, \sqsupset, \wp, \|\omega(k)\|_{max}$)
- 10 | /* Find paths with minimum cost */
- 11 *path* $\leftarrow \text{FindMinimumPath}(G, \mathbf{x}_{start}, \mathbf{x}_{end})$
- 12 **return** $\mathbf{u}(k)$

B. A*-based optimizer

A core component of the NRMPC scheme shown in Fig. 5 is its optimizer. The optimizer searches the control input space \mathbb{U} and the state space \mathcal{X} for a path that is optimal in terms of cost J_N . The choice of optimizer will decide the

quality of the returned path and subsequently determines the quality of the whole system. In this paper, we propose an A* algorithm for searching for an optimal trajectory.

It is proposed to utilize A* as a search tool for our NRMPC problem due to two primary reasons: (1) the search space can be cast into tree formats, whose root is the initial position and nodes are possible positions that the vehicle might obtain, and (2) A* finds the optimal solution for a graph or tree-based search problem in a computationally tractable manner. Algorithm 2 describes the A*-like method implemented for the NRMPC scheme.

Algorithm 2: Tree exploration based on A* search algorithm - ExploreTree()

Input: The tree $G = (V, E)$, \sqsupset and \wp lists, desired end node \mathbf{x}_{end} , $\|\omega(k)\|_{max}$, and $\mathcal{B}_{\bar{\eta}_f, r_f}$.

Output: Extended tree $G' = (V', E')$, \sqsupset' and \wp' lists, and (*flag*) for terminal constraint

- 1 $V' \leftarrow V; E' \leftarrow E$
- 2 **while** \sqsupset is not empty **do**
- 3 | /* Dequeue highest priority element */
- 4 | $\mathbf{x}_{min} \leftarrow \text{DequeueMinCostNode}(\sqsupset)$
- 5 | /* Propagation following constraints */
- 6 | $\mathbf{Z}_{prop} \leftarrow \text{PropagateNode}(\mathbf{z}_{min}, \|\omega(k)\|_{max})$
- 7 | /* Infer associated costs */
- 8 | $\text{costs} \leftarrow$
 $\text{InferNodeCost}(\mathbf{z}_{min}, \mathbf{Z}_{prop}, \|\omega(k)\|_{max})$
- 9 | /* Extend tree from dequeued node */
- 10 | $\mathbf{X}_{new} \leftarrow \text{Steer}(\mathbf{z}_{min}, \mathbf{Z}_{prop}, \text{costs})$
- 11 | /* Add new nodes to existing tree */
- 12 | $V' \leftarrow V' \cup \mathbf{X}_{new}; E' \leftarrow$
 $E' \cup \{(\mathbf{x}_{min}, \mathbf{X}_{new})\}; G' \leftarrow (V', E')$
- 13 | /* Put the explored node to CLOSED */
- 14 | $\wp' \leftarrow \mathbf{x}_{min}$
- 15 | /* Adding unexplored nodes to OPEN */
- 16 | $\sqsupset' \leftarrow \sqsupset; \sqsupset' \leftarrow \mathbf{X}_{new}$
- 17 **if** *CheckTerminalConstraint*(G') **then**
- 18 | /* Terminal constraint checking */
- 19 | *flag* $\leftarrow 1$
- 20 | $G' \leftarrow \text{MarkConvergence}(G')$
- 21 **else**
- 22 | *flag* $\leftarrow 0$
- 23 **return** G', flag

Once Algorithm 2 is activated, it initially, via the use of *DequeueMinCostNode*, selects a node \mathbf{x}_{min} which has the lowest cost amongst nodes in the \sqsupset list. *PropagateNode* then propagates coordinates \mathbf{z}_{min} of \mathbf{x}_{min} according to kinematics (4), input, and output constraints. All of the predicted states after state propagation process are represented by \mathbf{Z}_{prop} . The function *InferNodeCost* is then invoked so that costs of states in \mathbf{Z}_{prop} are evaluated according to (6), and (11). Finally, *Steer* creates a set of new nodes \mathbf{X}_{new} that contains both states and costs corresponding to \mathbf{Z}_{prop} . After predicting new nodes \mathbf{X}_{new} , the tree G , and \sqsupset and \wp lists are updated. Finally, the terminal constraint

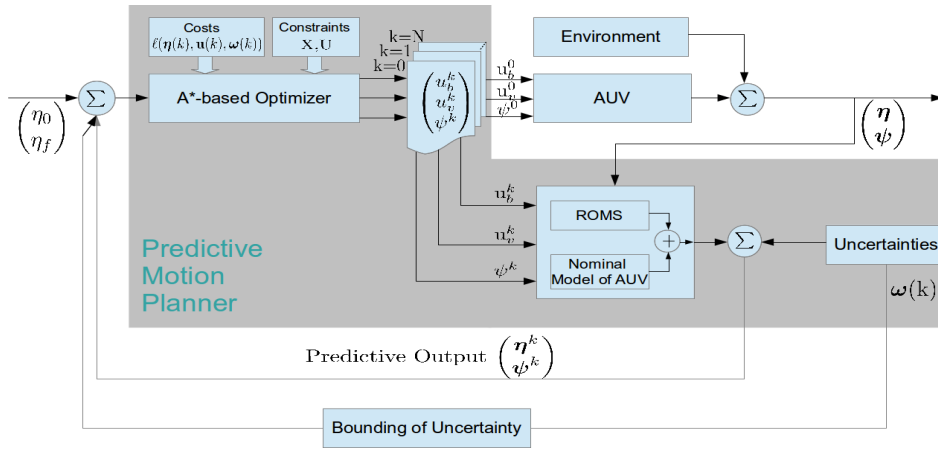


Fig. 5. A closed-loop block diagram depicting the operation of the NRMPC path planning and scheme with ocean current predictions.

is checked before exiting Algorithm 2. If there are nodes satisfying the terminal constraint, such nodes will be marked by *MarkConvergence* and *flag* is turned on.

The aim of A*-based algorithm is to find the optimum solution for the NRMPC problem, while minimizing any unnecessary exploration. The heuristic function $\ell_{heuristic}(k)$ (Eq. 10) is used for the search. The purpose of employing such an heuristic function is to guarantee that the heuristic cost $\ell_{heuristic}$ is lower than the actual cost $\ell_{heuristic}^*$ to travel from the current location to the destination, and thus optimality of the resultant path is ensued.

However, theoretical optimally computed paths can be difficult to implement in the field as the level of uncertainty may be high. Basically, near-optimal paths, that can sustain against uncertainty and be executed to arrive at the goal successfully, are normally expected in reality. Consequently, $\ell_{heuristic} > 0$ is chosen in such a way that makes the A*-based optimizer generates near-optimal, robust paths while maintaining the computation time sufficiently short, i.e., less than the sampling time T .

When cost of the chosen heuristic function is much lower than the actual cost, i.e., we are too optimistic about the cost to assume that $\ell_{heuristic} \ll \ell_{heuristic}^*$, then the computational efficiency of the search is degraded due to having to search many more paths.

In the current study, it is preferable to embrace a balanced approach between computational time and optimality. Here we applied trial and error method to tune E_{appr} of $\ell_{heuristic}$ so that near optimality occurs and computational time does not exceed the sampling time. If the search converges straight forward to the goal destination without stepping back, this is equivalent to $\ell_{heuristic} > \ell_{heuristic}^*$ and the search is similar to the greedy algorithm. We might then decrease $\ell_{heuristic}$. This results in increase of convergence time. If convergence time is greater than sampling time, it is highly likely that we are at the point of using too optimistic value for E_{appr} . Consequently, a proper value for E_{appr} might be taken to be an average of the “too-optimistic” point and the “greedy-algorithm-like” point.

The computational efficiency and tuning of the heuristic function, including online learning of this parameter are

avenues of future development.

Algorithms 1 and 2 formulate the forward path of the diagram in Fig. 5. The feedback path is implemented by the condition checking of the *while* loop in Algorithm 1. Consequently, combining Algorithms 1 and 2 implements the closed-loop NRMPC scheme in Fig. 5.

VI. RESULTS

Two scenarios of motion planning that takes into account uncertain forecasting of the time-varying ocean currents along (b_1, b_2, b_3) are presented. In the first case, we consider the scenario when the ocean model prediction (OMP) is perfect and deterministic. The second case is the scenario when ocean model prediction contains uncertainties (see [24] for information about uncertainty in OMP). The uncertainty bound in this study is derived from observation of historical ocean current predictions. Particularly, we consider the uncertainties varying to the upper bound $\|\omega\| \leq 0.4$ km/sample time, i.e., predictions of ocean currents spread within a square of side length 0.4 km.

A. Scenario 1: NRMPC path planning with deterministic ocean currents prediction

In Scenario 1, the ocean current prediction is assumed perfect in this case, $\omega = 0$. The absolute velocity of the AUV is set to $\|v_a\| = 2.5$ knots. The distance between starting point and the goal is approximately 10 km. The value of $E_{ht/sample}$ is set to 12 W/hour. The radius of $\mathcal{B}_{\eta_f, r}$ is $r_f = 10$ m.

Figure 6 shows the NRMPC derived optimal energy path starting from the cyan star and travelling to the red square. Figure 7 shows the associated switching of depths of AUV over the whole course of travel. In Fig. 6, the radiating lines in magenta represent the A* tree branch evolution during the search for solutions of the NRMPC scheme. Here, there were 16 possible heading angles (ψ) and 24 values of depths u_v giving a total of 384 possible evolutions of the AUV movement at each time step requiring consideration. Each of the possible evolutions corresponds to a branch of the tree.

The energy-optimal path in Fig. 6 is seen to deviate from the straight line trajectory so that the vehicle can exploit

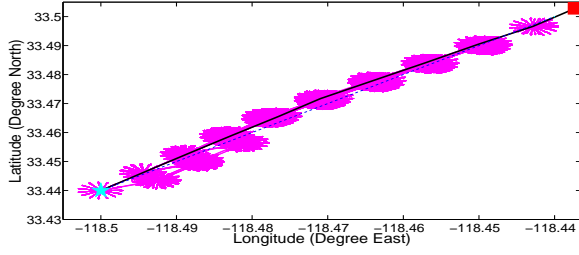


Fig. 6. Evolution of A* tree (in magenta) and the resultant planned path (in blue and continuous) starting from the cyan star to the red square. Total path length was approximately 10 km.

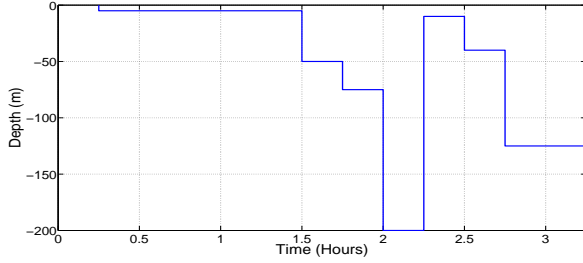


Fig. 7. Resultant depth trajectory of the planned path for the deterministic case shown in Figure 6.

ocean currents and save energy when traversing from the start position to the goal. The energy efficiency produced by the planned path is:

$$\begin{aligned}
 Eff_{path} &= \frac{E_{SL} - E_{NRMPC}}{E_{SL}} \times 100 \\
 &= \frac{73.09 - 53.59}{73.09} = 26.67\%, \quad (12)
 \end{aligned}$$

where E_{SL} is the energy required to travel along the straight-line trajectory, and E_{NRMPC} is the energy required to travel along the NRMPC path. The results show that in this case, the energy savings are considerable.

Here we see from Fig. 7 that at time $t = 2$ hours, the vehicle is at 200 m and is required to go to near the surface at the next time step. The assumption of instant depth traversal becomes less valid with greater inter-step depth changes. The influence of this assumption is a focus of future research.

B. Scenario 2: NRMPC path planning with uncertain ocean currents prediction

Figure 8 shows an example of the paths planned using NRMPC with varying levels of ocean forecast uncertainty ranging from 0 (nominal case), 0.1, 0.2 and 0.4 km / sample time. Here the same start and end points are used as for Figure 6. The NRMPC is run with a forecast horizon of $N = 8$. This forecast horizon was selected as a compromise between prediction and computational effort. Future research will evaluate the performance with increased horizon. To close the loop of the path planner, only $u(k, 0)$ is applied at each step and recalculated at the next epoch. The lower subfigure presents the optimised depth profile for each trajectory. The paths planned vary in space and time with the nominal path almost straight and paths which account for

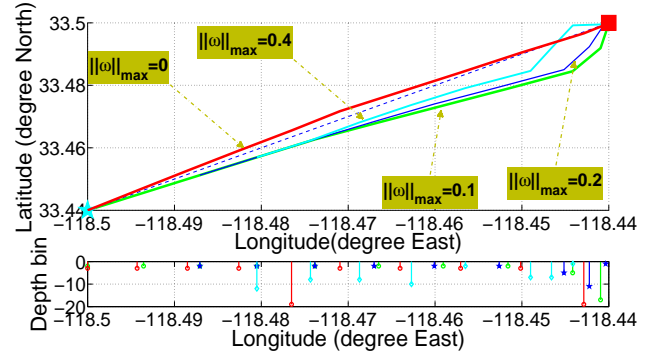


Fig. 8. Planned trajectories with existence of different forecasting uncertainties along the trajectory. The top figure shows the resultant planned paths in the horizontal plane with ocean forecast uncertainty 0 (red), 0.1 (green), 0.2 (blue) and 0.4 (cyan) km/sample time. The bottom figure shows the corresponding depth profile for each trajectory.

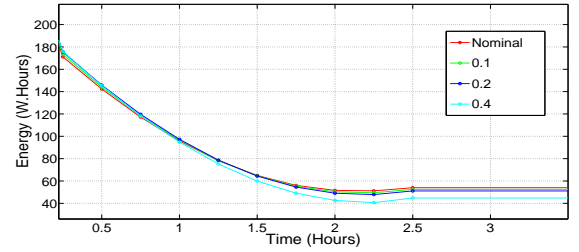


Fig. 9. Predicted total energy to complete the path with time for the AUV with nominal and uncertainty scenarios.

uncertainty showing more variability. However, in all cases they all converge to the goal point.

Figure 9 shows the predicted energy consumed by the AUV with time along the trajectories for each of the uncertainty cases shown in Fig. 8. The predicted energy at time (k) is defined as the actual energy expended up to time (k) and the predicted required energy to complete the path. The red line is expected energy for nominal case when there exists no uncertainty. The green, blue and red curves are expected energy for bounded uncertainties of (0.1, 0.2, 0.4) respectively. Table I shows the percentage of energy efficiency from the nominal case for each of the paths from Fig. 8.

	Nominal	$\ \omega\ _{max}$		
		0.1	0.2	0.4
SL	73.0951	73.1037	73.0923	73.0831
NRMPC	53.6	51.47	49.69	44.93
$Eff_{path}(\%)$	26.67	29.59	32.02	38.52

TABLE I

COMPARISON OF ENERGY SAVING FOR NOMINAL AND VARIOUS BOUNDED UNCERTAINTY CASES.

As can be seen in Fig. 9, the initial predicted energy is conservative and decreases with time for all cases. We see that the expected energy for scenarios with uncertainty is higher than that of the nominal case at the beginning of travel. However, in this case, as the vehicle move forward to the goal, the expected energy for the 0.4 uncertainty case

is less than that of the 0.1 case. This could be explained by observing the AUV expends more energy at the beginning to overcome uncertainties (the worst case prediction of ocean currents). As time progresses the vehicle may select a favourable current to the destination that assist the vehicle to use less energy. Additionally, with higher-uncertainties the NRMPC approach explores more of the region around the A* nodes. Therefore, it may detect more favourable currents than for lower uncertainty cases. It can be seen in Table I that in this case, the energy savings are greater with increasing uncertainty.

VII. CONCLUSION

This paper has presented a novel path planning algorithm for minimising the energy expenditure of the AUV in 4-D configuration space in the presence of both environmental disturbances and model uncertainties. Control inputs for the problems consist of not only the vehicle propulsion but also environmental forces. Resultant paths are optimal solutions of the nonlinear model predictive control problem whose optimizer is constructed based on an A* searching algorithm. Results show that the algorithm is able to produce energy-efficient paths while accommodating bounded model uncertainties. Future work will experimentally evaluate the planning performance with varying ocean current predictions and forecast uncertainties, as well as the relaxation of simplifying assumptions of vehicle dynamics.

ACKNOWLEDGEMENTS

V. Huynh was supported by QUTPRA scholarship from the Queensland University of Technology. R.N. Smith was supported in part by a Byron Dare Junior Faculty Award.

REFERENCES

- [1] G. Griffiths, Ed., *Technology and Applications of Autonomous Underwater Vehicles*. Taylor & Francis, 2003.
- [2] R. Marthiniussen, K. Vestgard, R. Klepaker, and N. Storkersen, "Hugin-AUV concept and operational experiences to date," in *MTTS/IEEE TECHNO-OCEAN '04*, vol. 2, Nov 2004, pp. 846–850 Vol.2.
- [3] P. Hagen, N. Storkersen, B.-E. Marthinsen, G. Sten, and K. Vestgard, "Military operations with Hugin AUVs: lessons learned and the way ahead," in *Oceans 2005 - Europe*, vol. 2, June 2005, pp. 810–813 Vol. 2.
- [4] E. Fernandez-Perdomo, J. Cabrera-Gamez, D. Hernandez-Sosa, J. Isern-Gonzalez, A. Dominguez-Brito, A. Redondo, J. Coca, A. Ramos, E. Fanjul, and M. Garcia, "Path planning for gliders using regional ocean models: Application of Pinzon path planner with the ESEOAT model and the RU27 trans-Atlantic flight data," in *IEEE OCEANS 2010 - Sydney*, May 2010, pp. 1–10.
- [5] K. Dahl, D. Thompson, D. McLaren, Y. Chao, and S. Chien, "Current-sensitive path planning for an underactuated free-floating ocean sensorweb," in *Proceedings of IEEE International Conference on Intelligent Robots and Systems*, Sept 2011, pp. 3140–3146.
- [6] J. Isern-Gonzalez, D. Hernandez-Sosa, E. Fernandez-Perdomo, J. Cabrera-Gamez, A. Dominguez-Brito, and V. Prieto-Maranon, "Path planning for underwater gliders using iterative optimization," in *Robotics and Automation (ICRA), 2011 IEEE International Conference on*, May 2011, pp. 1538–1543.
- [7] J. Witt and M. Dunbabin, "Go with the flow: Optimal AUV path planning in coastal environments," in *Proceedings of the Australasian Conference on Robotics and Automation*, J. Kim and R. Mahony, Eds., Canberra, ACT, 2008, ISBN: 9780646506432.
- [8] I. P. King, "Update documentation: Rma2 - a two-dimensional finite element model for flow in estuaries and streams," Resource Modelling Associates, Sydney, Australia, Tech. Rep., 2004.
- [9] B. Garau, A. Alvarez, and G. Oliver, "Path planning of autonomous underwater vehicles in current fields with complex spatial variability: an A* approach," in *Proceedings of the IEEE International Conference on Robotics and Automation*, april 2005, pp. 194 – 198.
- [10] K. Carroll, S. McClaran, E. Nelson, D. Barnett, D. Friesen, and G. William, "AUV path planning: an A* approach to path planning with consideration of variable vehicle speeds and multiple, overlapping, time-dependent exclusion zones," in *Proceedings of the Symposium on Autonomous Underwater Vehicle Technology*, Jun 1992, pp. 79–84.
- [11] T.-B. Koay and M. Chitre, "Energy-efficient path planning for fully propelled AUVs in congested coastal waters," in *MTS/IEEE OCEANS - Bergen*, June 2013, pp. 1–9.
- [12] T. Lolla, P. Lermusiaux, M. Ueckermann, and J. Haley, PatrickJ., "Time-optimal path planning in dynamic flows using level set equations: theory and schemes," *Ocean Dynamics*, vol. 64, no. 10, pp. 1373–1397, 2014.
- [13] A. Alvarez, A. Caiti, and R. Onken, "Evolutionary path planning for autonomous underwater vehicles in a variable ocean," *IEEE Journal of Oceanic Engineering*, vol. 29, no. 2, pp. 418–429, 2004.
- [14] C. Petres, Y. Pailhas, P. Patron, Y. Petillot, J. Evans, and D. Lane, "Path planning for autonomous underwater vehicles," *Robotics, IEEE Transactions on*, vol. 23, no. 2, pp. 331 –341, april 2007.
- [15] D. Kruger, R. Stolkin, A. Blum, and J. Briganti, "Optimal AUV path planning for extended missions in complex, fast-flowing estuarine environments," in *Proceedings of IEEE International Conference on Robotics and Automation*, Rome, Italy, 2007.
- [16] B. Garau, M. Bonet, A. Alvarez, S. Ruiz, and A. Pascual, "Path planning for autonomous underwater vehicles in realistic oceanic current fields: Application to glider in the Western Mediterranean Sea," *Maritime Research*, vol. 6, pp. 5–22, 2009.
- [17] M. Soulignac, "Feasible and optimal path planning in strong current fields," *Robotics, IEEE Transactions on*, vol. 27, no. 1, pp. 89–98, Feb 2011.
- [18] W. Al-Sabban, L. Gonzalez, and R. Smith, "Wind-energy based path planning for unmanned aerial vehicles using Markov decision processes," in *Proceedings of IEEE International Conference on Robotics and Automation*, May 2013, pp. 784–789.
- [19] A. A. Pereira, J. Binney, G. A. Hollinger, and G. S. Sukhatme, "Risk-aware path planning for autonomous underwater vehicles using predictive ocean models," *Journal of Field Robotics*, vol. 30, no. 5, pp. 741–762, 2013.
- [20] L. Grune and J. Pannek, *Nonlinear Model Predictive Control: Theory and Algorithms*, 2011.
- [21] S. Heshmati-Alamdari, A. Eqtami, G. C. Karras, D. V. Dimarogonas, and K. J. Kyriakopoulos, "A self-triggered visual servoing model predictive control scheme for underactuated underwater robotic vehicles," in *Proceedings of International Conference on Robotics and Automation*, 2014.
- [22] A. F. Shchepetkin and J. C. McWilliams, "The Regional Oceanic Modeling System (ROMS): a split-explicit, free-surface, topography-following-coordinate oceanic model," *Ocean Modelling*, vol. 9, no. 4, pp. 347–404, 2005.
- [23] Z. Li, Y. Chao, J. C. McWilliams, and K. Ide, "A three-dimensional variational data assimilation scheme for the regional ocean modeling system," *Journal of Atmospheric and Oceanic Technology*, vol. 25, no. 11, pp. 2074–2090, 2008.
- [24] R. N. Smith, J. Kelly, K. Nazarzadeh, and G. S. Sukhatme, "An investigation on the accuracy of regional ocean models through field trials," in *Proceedings of the IEEE International Conference on Robotics and Automation*, 2013.
- [25] J. Acevedo and E. N. Pistikopoulos, "A multiparametric programming approach for linear process engineering problems under uncertainty," *Industrial & Engineering Chemistry Research*, vol. 36, no. 3, pp. 717–728, 1997.
- [26] J. Löfberg, "Yalmip : A toolbox for modeling and optimization in MATLAB," in *Proceedings of the CACSD Conference*, Taipei, Taiwan, 2004. [Online]. Available: <http://users.isy.liu.se/johanl/yalmip>
- [27] M. Kvasnica, P. Grieder, and M. Baotić, "Multi-parametric toolbox (mpt)," 2004. [Online]. Available: <http://control.ee.ethz.ch/~mpt/>
- [28] H. Choset, K. M. Lynch, S. Hutchinson, G. Kantor, W. Burgard, L. E. Kavraki, and S. Thrun, *Principles of Robot Motion: Theory, Algorithms, and Implementations*. MIT Press, Boston., 2005.